CrossMark

ORIGINAL PAPER

Synthesis and Preparation of Magnetic Fe-Doped CeO$_2$ Nanoparticles Prepared by Simple Sol-Gel Method

M. Dastpak[1] · M. Farahmandjou[1] · T. P. Firoozabadi[1]

Abstract Fe-doped ceria nanoparticles were synthesized by a simple co-precipitation method via iron nitrate (Fe(NO$_3$)$_3$·9H$_2$O) and cerium nitrate (Ce(NO$_3$)$_3$·6H$_2$O) as a precursor in the presence of diethylene glycol and ammonia solution. The prepared samples were characterized by high-resolution transmission electron microscopy (HRTEM), field effect scanning electron microscopy (FESEM), X-ray diffraction (XRD), vibration sampling magnetometer (VSM), and Fourier transform infrared spectroscopy (FTIR) in different temperatures. The XRD results showed a cubic structure of Fe-doped CeO$_2$. The mean particle size of the as-prepared samples was around 30 nm, and that of samples annealed at 500 °C for 3 h was 35 nm. This analysis also indicated the change of particles to rod-like shape by increasing temperature. The TEM studies exhibited the square-like shaped nanoparticles. The sharp peaks in the FTIR spectrum determined the element of Fe–Ce nanoparticles. The magnetic measurements of the as-prepared samples showed a coercive field and saturation magnetism at about 1611 G and 0.06 emu/g, respectively.

Keywords Iron/ceria · Nanoparticles · EG agent · Sol-gel synthesis

✉ M. Farahmandjou
farahmandjou@iauvaramin.ac.ir

[1] Department of Physics, Islamic Azad University, Varamin Pishva Branch, Varamin, Iran

1 Introduction

Cerium oxide (CeO$_2$)-containing materials have been a focus of intensive research during the last years due to the diversity of their applications. Cerium oxide with different valence states and various crystalline structures has been explored for various applications such as electrical, electronic, catalytic, adsorption, optical, electrochemical, batteries, functional materials, energy storage, magnetic data storage, and sensing properties [1–9].

CeO$_2$ is a large bandgap semiconductor with an optical indirect bandgap of 3.20 eV [10], which limits its application within the ultraviolet (UV) radiation range. In order to reduce the bandgap and to enhance the photoactivity of CeO$_2$, transition metal ions of variable valency have been introduced into the CeO$_2$ lattice such as iron (Fe) [11], copper (Cu) [12], nickel (Ni) [13], manganese (Mn) [14], cobalt (Co) [15], and silver (Ag) [16]. Of these ions, iron is considered to be one of the most promising candidates, since Fe^{+3} can easily substitute for Ce ions or enter the interstices of the crystal lattice of CeO$_2$ [17], leading to the creation of donor or acceptor levels between the valence and conduction bands [18]. However, the crystallite size depends on the iron doping concentration. Indeed, the iron doping caused a decrease in the mean crystallite size. One possible explanation for this decrease is the fact that, before insertion into the CeO$_2$ structure, the dopant element is first likely located between the grain boundaries and consequently disturbs the growth kinetics of the crystallites. It is possible that doping Fe^{3+} can forbid the crystal growth. With higher concentrations of Fe^{3+}, it would possibly increase the blockade of crystal growth, giving rise to a decrease in particle size. The

same behavior was found in nanoparticles of TiO_2 that prohibit the growth in the [001] direction after Fe doping [19]. They reported that Fe^{3+} on the surface can form effective pathways for interfacial charge transfer for increasing the photocatalytic activity of TiO_2. As a result of this, Fe^{3+} is on the surface of spherical aggregates due to the small particle size, which is beneficial for increasing the magnetic interaction of Fe-doped CeO_2 nanospheres. Transition metal nanoparticles are of continuing interest because of their fascinating catalytic, electronic, and optical properties. These ultrafine particles often agglomerate to form either lumps or secondary particles in order to minimize the total surface or the interfacial energy of the system. Therefore, it is very important to stabilize the particles against adverse agglomeration at both the synthesis and the usage stages. It is well known that the type of stabilizer that is used to cap the nanoparticles affects their stability and, in turn, affects its catalytic activity [20–22]. A rigid surfactant surface layer tends to resist opening; thus, the reaction is slowed down and simultaneous nucleation and growth occur. This, in turn, results in the formation of large nanoparticles with broad size distribution. The main effect of stabilizers on particle size may be due to the steric effect and chemical bonding [23]. Several techniques have been used to prepare CeO_2 nanoparticles, including hydrothermal synthesis [24], homogeneous precipitation [25], sonochemical synthesis [26], and flame spray pyrolysis [27]. In this article, Fe–Ce magnetic nanoparticles were synthesized using iron nitrate and cerium nitrate precursors. Structural and surface morphological properties are discussed by X-ray diffraction (XRD), HRTEM, field emission scanning electron microscopy (FESEM), vibration sampling magnetometer (VSM), and Fourier transform infrared spectroscopy (FTIR) analyses.

2 Experimental Detail

Square-like shaped Fe/CeO_2 was synthesized by a simple synthesis method as follows. Initially, 2.5 g $Fe(NO_3)_3 \cdot 9H_2O$ and 10 ml diethylene glycol were dissolved into 50 ml pure water. After vigorous magnetic stirring for 10 min, 2.5 g $Ce(NO_3)_3 \cdot 6H_2O$ was added to the solution while stirring at room temperature. After 5 min, 10 ml ammonia solution was slowly added to the red-colored solution and the synthesis temperature was increased to 90 °C. A pH of 12 was maintained during the synthesis. The product was evaporated for 1.5 h, cooled to room temperature, and finally calcined at 500 °C for 3 h. All analyses were done for samples without any washing and purification.

The size, structure, and optical properties of as-synthesized and annealed nanoparticles were carried out. X-ray diffractometer was used to identify the crystalline phase and to estimate the crystalline size. The XRD pattern was recorded with 2θ in the range of 4–85° with type X'Pert Pro MPD, Cu-K$_\alpha$: $\lambda = 1.54$ Å. The morphology was characterized by FESEM with type KYKY-EM3200 (25 kV) and transmission electron microscopy (TEM) with type Zeiss EM-900 (80 kV). FTIR was performed with WQF 510. Magnetic measurements were carried out using the vibration sampling magnetometer with type VSM 7400 (Lake Shore). All the measurements were carried out at room temperature.

3 Results and Discussion

XRD analysis was used to identify crystalline phases and to estimate the crystalline sizes. Figure 1 shows the X-ray diffraction patterns of the powder before and after heat treatment. Figure 1a shows the XRD pattern of the iron ceria sample before annealing. Figure 1b shows the XRD patterns
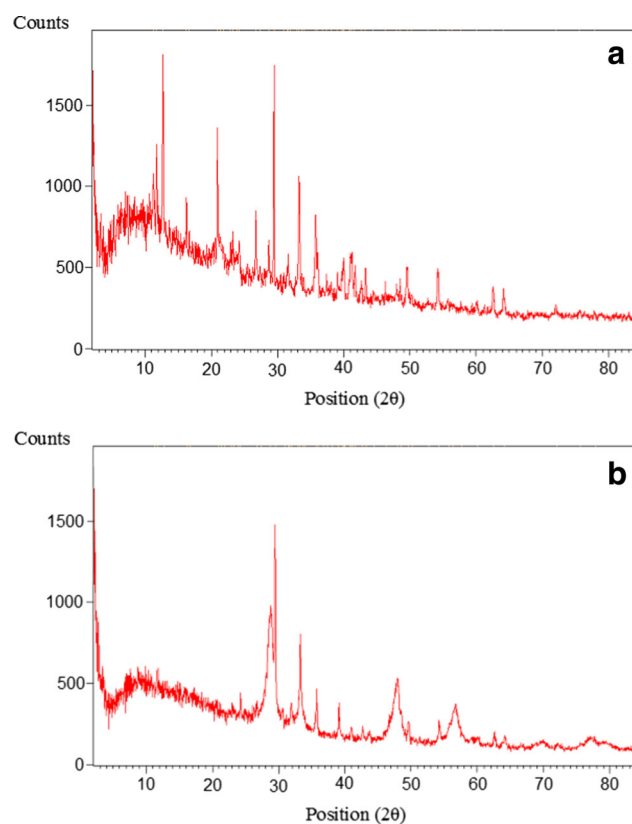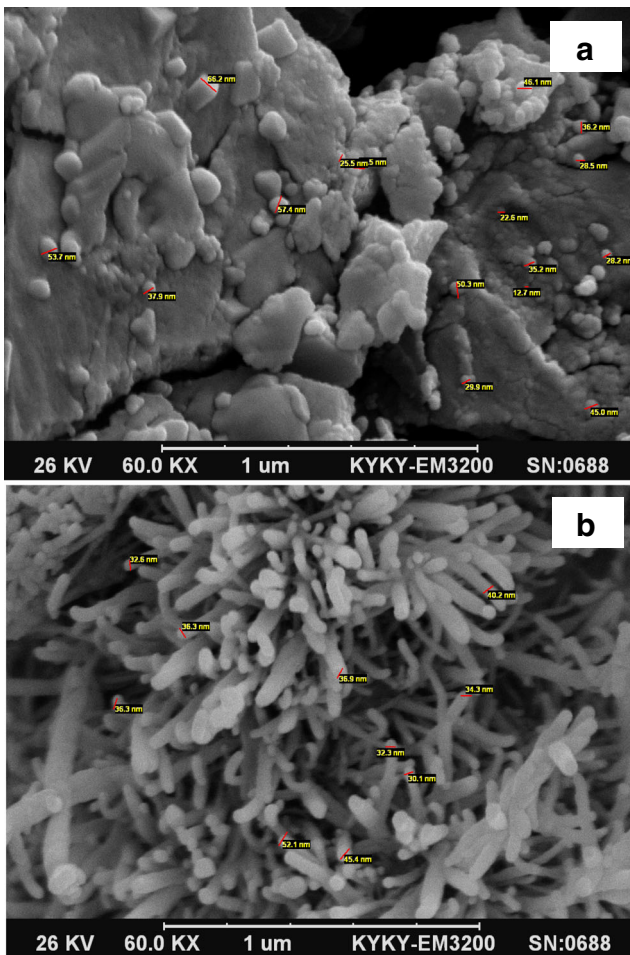

Fig. 1 XRD patterns of the as-prepared (**a**) and annealed (**b**) Fe–Ce samples

of iron cerium after annealing at 500 °C for 3 h. The exhibited peaks correspond to the cubic structure. The mean size of ordered Fe–Ce nanoparticles has been estimated from the full width at half maximum (FWHM) and Debye-Scherrer formula according to the following equation:
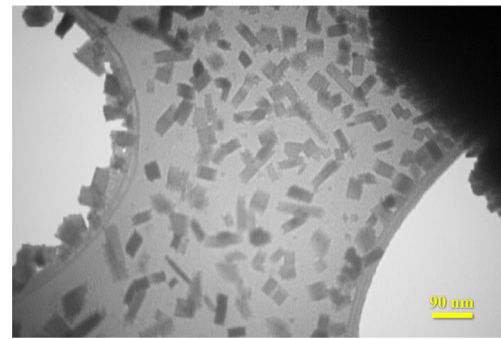
$$D = \frac{0.89\lambda}{B \cos \theta} \tag{1}$$

where 0.89 is the shape factor, λ is the X-ray wavelength, B is the line broadening at FWHM in radians, and θ is the Bragg angle. The mean size of 30 nm was estimated for the as-prepared samples from this Debye-Scherrer equation.

The morphology and structure of the Fe-doped CeO_2 samples were investigated by SEM as shown in Fig. 2. These analyses show the high crystallinity emerged in the samples' surface by increasing the annealing temperature. With increasing temperature, the nanoparticles changed from a sphere-like shape to rod-like shape with a diameter of 35 nm. Figure 2a shows the SEM image of the as-prepared
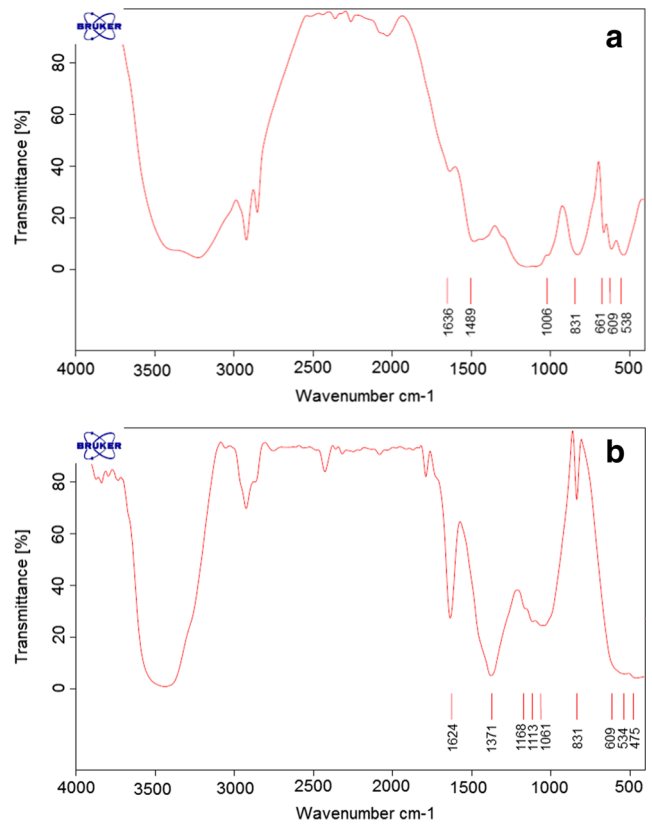

Fig. 3 TEM image of the as-prepared Fe–Ce nanoparticles

Fe–Ce nanoparticles prepared by this method. In this figure, the particles are formed with clusters. Figure 2b shows the SEM image of the annealed Fe–Ce nanoparticles at 500 °C for 3 h. The mean diameter of as-prepared nanoparticles was around 30 nm, and that of samples annealed at 500 °C for 3 h was 35 nm.

TEM analysis was carried out to confirm the actual size of the particles, their growth pattern, and the distribution of the crystallites. Figure 3 shows the as-synthesized TEM
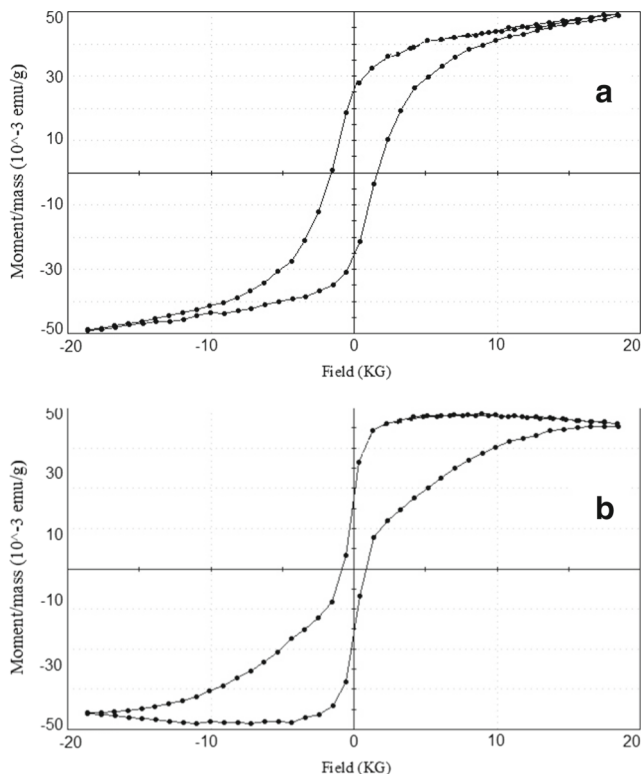

Fig. 2 SEM images of the as-prepared (**a**) and annealed at 500 °C (**b**) Fe–Ce nanoparticles

Fig. 4 FTIR spectrums of the as-prepared (**a**) and annealed (**b**) Fe–Ce samples
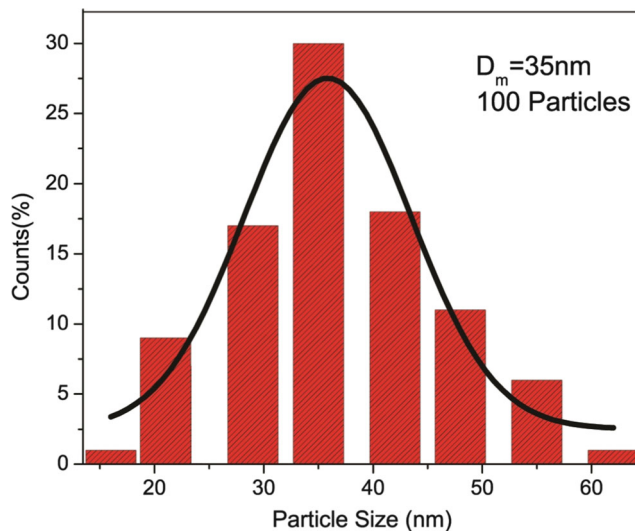
image of square-like shaped Fe–Ce nanoparticles, with an average diameter of 35 nm prepared by a chemical synthesis route.

In Fig. 4, the infrared spectrum (FTIR) of the as-synthesized and annealed Fe–Ce nanoparticles was in the range of 400–4000 cm^{-1} wavenumber which identify the chemical bonds as well as functional groups in the compound. For the as-prepared sample in Fig. 4a, the large broad band at 3450 cm^{-1} is ascribed to the O–H stretching vibration in OH$^-$ groups. The absorption peaks around 1632 cm^{-1}, and peaks at 1450 cm^{-1} are due to the asymmetric and symmetric bending vibration of C=O. The strong band below 700 cm^{-1} is assigned to Fe–Ce stretching mode. The bands corresponding to Fe–Ce stretching mode are seen at 586 and 482 cm^{-1}. For the annealed samples in Fig. 4b, the bands corresponding to Fe–Ce stretching mode are seen at 609, 534, and 475 cm^{-1}.

The magnetization (M) versus the applied magnetic field (H) for powders of the samples is measured at room temperature by cycling the magnetic field between -20 k and 20 kG. The magnetization curve in Fig. 5 shows the hysteresis behavior in the low field region. Figure 5a shows the coercive field and saturation magnetism around 1611 G and 0.06 emu/g for the as-prepared sample. Figure 5b exhibits the coercive field and saturation magnetization

Fig. 6 Particle diameter histogram of the as-prepared Fe–Ce nanoparticles

around 850 G and 0.08 emu/g, respectively, for the annealed one. It is also seen that the coercive field decreases with the annealing temperature.

Figure 6 shows the size measurement of 100 randomly selected particles. Fitting it with a log normal curve leads to a measured mean diameter of 35 nm with a standard deviation of about 9 %.

4 Conclusion

Fe-doped ceria nanoparticles have been successfully synthesized using iron nitrate and cerium nitrate in the presence of diethylene glycol and ammonia solution agents. The XRD spectrum exhibited a cubic structure of the samples. SEM images showed the change of particles to rod-like shape by increasing the temperature with less agglomeration. The TEM image of the sample indicated an Fe–Ce nanoparticle with an average diameter of 35 nm with good uniformity. The FTIR spectrum confirmed the presence of Fe–Ce stretching mode. The magnetic measurements of the as-prepared samples showed a coercive field and saturation magnetism at about 1611 G and 0.06 emu/g, respectively.

Fig. 5 VSM analyses of the as-prepared (**a**) and annealed at 500 °C (**b**) Fe–Ce nanoparticles

References

1. Faisal, M., Khan, S.B., Rahman, M.M., Jamal, A.: J. Mater. Sci. Technol. **27**, 549 (2011)

2. Faisal, M., Khan, S.B., Rahman, M.M., Jamal, A.: Chem. Engineer. J. **173**, 178 (2011)
3. Khan, S.B., Faisal, M., Rahman, M.M., Jamal, A.: Sci. Tot. Environ. **409**, 2987 (2011)
4. Niu, F., Zhang, D., Shi, L., He, X., Li, H., Mai, H., Yan, T.: Mater. Lett. **63**, 2132 (2009)
5. Palard, M., Balencie, J., Maguer, A., Hochepied, J.F.: Mater. Chem. Phys. **120**, 79 (2010)
6. Rao, G.R., Kaspar, J., Meriani, S., Monte, R., Graziani, M.: Cataly. Lett. **24**, 107 (1994)
7. Phokha, S., Pinitsoontorn, S., Maensiri, S.: Nano-Micro Lett. **5**(4), 223 (2013)
8. Almeida, J.M.A., Santos, P.E.C., Cardoso, L.P., Meneses, C.T.: J. Magn. Magn. Mater. **327**, 185 (2013)
9. Ansari, A., Labis, J., Alam, M., Ramay, S.M., Ahmad, N., Mahmood, A.: J. Chin. Chem. Soc. **62**, 925 (2015)
10. Hay, P.J., Martin, R.L., Uddin, S.J.G.E.: J. Chem. Phys. **25**, 034712 (2006)
11. Ye, W.Q., Wu, Z.H., Hui, Y.Q., Sheng, L., Gang, X.D., Quan, T.J.: Chin. Phys. Lett. **26**, 047803 (2009)
12. Neiva, L.S., Leal, E., MeloCosta, A.C.F., Mascarenhas, A.J.S., Andrade, H.M.C., Gama, L.: Mater. Sci. Forum **899**, 660–661 (2010)
13. Kumar, S., Kim, Y.J., Koo, B.H., Lee, C.G.: J. Nanosci. Nanotech. **10**, 7204 (2010)
14. Santos, E.L., Muccillo, R., Muccillo, E.N.S.: Mater. Sci. Forum. **639**, 591–593 (2008)
15. Kumar, S., Kim, Y.J., Koo, B.H., Choi, H., Lee, C.G.: IEEE Trans. Magn. **45**, 2439 (2009)
16. Kitiwiang, C., Phanichphant, S.: J. Micro. Soc. Thailand **23**, 83 (2009)
17. Liang, C., Ma, Z., Lin, H., Ding, L., Qiu, J., Frandsen, W., Su, D.: J. Mater. Chem. **19**, 1417 (2009)
18. Wang, Z., Quan, Z., Lin, J.: Inorganic Chemi. **43**, 5237 (2007)
19. Wen, L., Liu, B., Zhao, X., Nakata, K., Murakami, T., Fujishima, A.: Int. J. Photoenergy **2012**, 368750 (2012)
20. Roucoux, A., Schulz, J., Partin, H.: Am. Chem. Soc. **102**, 3757 (2002)
21. Kishore, P.S., Viswanathan, B., Varadarajan, T.K.: Nanoscale Res. Lett. **3**, 14 (2008)
22. Miyazaki, A., Balint, I., Nakano, Y.: J. Nanopart. Res. **5**, 69 (2003)
23. Tu, W.X.: Chinese J. Poly. Sci. **26**, 23 (2008)
24. Masui, T., Hirai, H., Imanaka, N.: J. Mater. Sci. Lett. **21**, 489 (2004)
25. Chen, H.I., Chang, H.Y.: Colloids. Surf. A **242**, 61 (2004)
26. Yin, L.X., Wang, Y.Q., Pang, G.S., Koltypin, Y., Gedanken, A.: J. Colloid. Interface. Sci. **246**, 78 (2002)
27. Gojova, A., Lee, J.T., Jung, H.S., Guo, B., Barakat, A.I., Kennedy, I.M.: Inhalation Tox. **21**, 123 (2009)